# Calibration of SAR Polarimetric Images by Means of a Covariance Matching Approach

Alberto Villa, Lorenzo Iannini, Davide Giudici, Andrea Monti-Guarnieri, *Member, IEEE*, and Stefano Tebaldini

## I. Introduction

RADAR polarimetry allows the collection of a significant wealth of information, with respect to single-channel synthetic aperture radar (SAR) sensors, at the expense of greater system complexity. Polarimetric calibration is a necessary preprocessing step for the correction of distortion interference due to system inaccuracies and atmospheric effects.

The problem can be approached from two different application angles: by a system monitoring viewpoint, when the estimation of system distortion parameters such as crosstalks (CTs) and channel imbalances (CIs) is targeted, and by an image calibration standpoint, where the efforts are not aimed at retrieving the parameters, rather at removing the joint distortion effect on the data. In either case, it is necessary to rely on some reference calibrator. Both the use of distributed targets (DTs) alone and in combination with one or more calibrators, such as trihedral corner reflectors (CRs) and polarimetric active radar calibrators (PARCs), have been considered in the literature [1]–[3]. The former solution would appear as the most convenient one since it avoids the deployment of artificial reflectors. However, the limited amount of information provided by a DT poses relevant challenges for the accurate estimation of the parameters, and the use of known point targets is required for complete system monitoring.

Calibration approaches relying exclusively on DT were conceived almost simultaneously with the ones based on calibrated reflectors and were tested on airborne campaigns in preparation for the SIR-C mission. Sarabandi *et al.* [4] was one of the first to propose effective DT-based calibration, robust to noise contribution, with the drawback that a good knowledge of the target scattering matrix is required. Quegan proposed in [1] a method exploiting the characteristics of a DT to perform parameter monitoring without the knowledge of the DT scattering matrix. The method was able to provide a full calibration up to a complex factor representing a CI, which could not be solved. An iterative least squares solution of the problem, based on the initial estimates of the Quegan method, was proposed in [5] to increase the estimation accuracy of the equivalent CT parameters, leading to improvements when the ratio HH/HV is between 5 and 15 dB. A second improvement was presented in [6]. In case of large differences between the noise affecting the polarimetric channels (for example, in case of damages of the sensor electronics), the method provides a refined estimate of the CI ratio. However, the use of a DT only appears inadequate for system monitoring since single CI cannot be estimated, rather only their ratio, unless the DT scattering values are known.

The influence of the Ionosphere, which can be neglected for airborne systems and high-frequency-band sensors, poses further challenges for polarimetric calibration. The launch of new satellites at L-band (such as the Argentinean sensor SAOCOM and the Japanese Advanced Land Observing Satellite ALOS II) makes the ionospheric influence retrieval essential to provide a correct calibration [7]. Even if several works have addressed the rotation introduced by the Ionosphere (see, for example, the comparative studies [8] and [9]), the joint estimation of system nonidealities and Faraday rotation angle (FRA) introduced by the Ionosphere is an open point. Several solutions have been proposed, even if limitations are posed by the assumptions done. The possibility to obtain an analytical solution of the system by using a DT only, in the case of symmetric system CTs and small FRA values, was presented in [10]. The technique gives consistent results for small, but not null, values of FRA so that the assumption of the technique is not violated. However, recent studies showed that in modern antenna arrays, the CTs cannot be considered as symmetric, with differences reaching up to several decibels (see, for example, [3] and [11]). Moreover, at solar maximum activity, 75% of an L-band satellite orbit is affected by FRA larger than 5° [12].

Manuscript received November 11, 2013; revised March 26, 2014 and May 13, 2014; accepted May 21, 2014.

A. Villa, D. Giudici, and A. Monti-Guarnieri are with Advanced Remote Sensing System (Aresys), Politecnico di Milano, 20134 Milan, Italy (e-mail: alberto.villa@aresys.it; davide.giudici@aresys.it; monti@elet.polimi.it).

L. Iannini is with the Department of Geoscience and Remote Sensing, Delft University of Technology, 2628 CN Delft, The Netherlands (e-mail: L.Iannini@tudelft.nl).

S. Tebaldini is with the Politecnico di Milano, 20133 Milan, Italy (e-mail: tebaldini@elet.polimi.it).

Color versions of one or more of the figures in this paper are available online.

The use of active calibrators such as PARCs has been investigated in several studies (both for high- [3] and low-frequency [13] systems): Transponders offer good quality at the expense of a larger cost of deployment and maintenance. Because of this reason, we focus our attention on the use of CRs, which are cheaper, easier to maintain, and provide a higher cross-polarization isolation. Moreover, a large number of CRs have been already deployed for past missions and could be eventually reused for new ones.

Freeman proposed in [14] a technique to estimate CIs and Faraday rotation. The author recognizes that significant correlations between like- and cross-polarized measurements can be caused by small FRAs, which will dominate those caused by CTs. The technique [14] assumes that CTs are low enough to be neglected or already calibrated before FRA estimation. The estimation of both CTs and Faraday rotation was proposed by Touzi and Shimada in [2], where passive CRs were considered, and Shimada in [11], with the use of rainforest plus CRs. In both cases, the ambiguity existent between CTs and FRA was solved by proposing some *a priori* assumptions, particularly the possibility to have an image with null Faraday rotation, in order to characterize the system polarimetric distortion contributions. Notice that this requires the stability of amplitude and phase of system distortion contributions.

Takeshiro *et al.* proposed in [15] a method that exploits two different point targets, i.e., a trihedral reflector as a polarization preserving reflector and a twisted reflector as a polarization rotating one. The method provides an estimate of the FRA by assuming that the CTs are null, which avoids approaching the intrinsic ambiguity. This ambiguity cannot be ignored when they try to derive the CTs, and the authors state that the method is not applicable when the FR angle is as small as the order of antenna CT factors.

In conclusion, a large number of techniques stated the difficulty in the joint estimation of CTs and Faraday rotation. However, at the authors' best knowledge, little effort has been posed in the possibility to estimate the full polarimetric distortion model through a model analysis. The methods proposed for system monitoring are generally limited by the assumptions done regarding the presence/absence of Faraday rotation or about its value. The first contribution of this work is the evaluation of the conditioning of the linearized forward model. We identify the ambiguity of the nonlinear problem, and we provide a model to evaluate the achievable accuracy for each parameter. Once the conditions under which the problem can be solved are found, we propose a numerical optimizer based on a COvariance Matching Estimation Technique (COMET) [16] to estimate the distortion parameters.

COMET provides a numerical approach that is optimal in statistical sense and suited to take advantage of all the information available, such as DT and CR. It has been already exploited with success in SAR-related fields, for example, for the polarimetric decomposition of interferometric SAR stacks [17]. The COMET cost function has been considered for detection since it has been proven that it guarantees results comparable or better than the generalized maximum-likelihood ratio index [16]. The accuracy of the method and the convergence are evaluated on simulated data. Real data from ALOS PALSAR are used to assess the robustness of the approach. The remainder of this paper is as follows. Section II provides a general overview of the polarimetric distortion problem, whereas Section III presents the numerical optimizer considered in this paper. The experiments on simulated and real data are shown in Sections IV and V, and conclusions are drawn in Section VI.

## II. Polarimetric Distortion Problem

The polarimetric distortion problem can be illustrated in a first approximation by the following equation [14]:

$$\begin{bmatrix} M_{\mathrm{HH}} & M_{\mathrm{HV}} \\ M_{\mathrm{VH}} & M_{\mathrm{VV}} \end{bmatrix} = A \cdot \begin{bmatrix} 1 & \delta_2 \\ \delta_1 & f_1 \end{bmatrix} \cdot \begin{bmatrix} \cos\Omega & -\sin\Omega \\ \sin\Omega & \cos\Omega \end{bmatrix} \cdot \begin{bmatrix} S_{\mathrm{HH}} & S_{\mathrm{HV}} \\ S_{\mathrm{VH}} & S_{\mathrm{VV}} \end{bmatrix} \cdot \begin{bmatrix} \cos\Omega & -\sin\Omega \\ \sin\Omega & \cos\Omega \end{bmatrix} \cdot \begin{bmatrix} 1 & \delta_3 \\ \delta_4 & f_2 \end{bmatrix} + \begin{bmatrix} N_{\mathrm{HH}} & N_{\mathrm{HV}} \\ N_{\mathrm{VH}} & N_{\mathrm{VV}} \end{bmatrix} \tag{1}$$

where $M_{pq}$ is the measured signal for the polarization $pq$, $A$ is the radiometric calibration factor, $\delta_x$ are the system CTs, $f_x$ are the CIs, $\Omega$ is the FRA, and $S_{pq}$ is the target scattering value for the polarization $pq$. We can write in a compact form

$$\mathbf{M} = A \cdot \mathbf{R^T} \cdot \mathbf{R_F} \cdot \mathbf{S} \cdot \mathbf{R_F} \cdot \mathbf{T} + \mathbf{N} \tag{2}$$

corresponding the matrix to the elements listed in (1). Term A is assumed real, i.e., we ignore an overall phase term that cannot be usually retrieved by a single polarimetric image. The distortion due to transmission and receiving contributions can be compacted in a single matrix, i.e., the polarimetric distortion matrix (PDM). Let us vectorize the observation and target scattering and noise, respectively, as

$$\vec{\mathbf{M}} = \begin{bmatrix} M_{\mathrm{HH}} \\ M_{\mathrm{HV}} \\ M_{\mathrm{VH}} \\ M_{\mathrm{VV}} \end{bmatrix} \quad \vec{\mathbf{S}} = \begin{bmatrix} S_{\mathrm{HH}} \\ S_{\mathrm{HV}} \\ S_{\mathrm{VH}} \\ S_{\mathrm{VV}} \end{bmatrix} \vec{\mathbf{N}} = \begin{bmatrix} N_{\mathrm{HH}} \\ N_{\mathrm{HV}} \\ N_{\mathrm{VH}} \\ N_{\mathrm{VV}} \end{bmatrix}. \tag{3}$$

We can rewrite (1) in a more convenient way as follows:

$$\vec{\mathbf{M}} = A \cdot \mathbf{H} \cdot \vec{\mathbf{S}} + \vec{\mathbf{N}} \tag{4}$$

where $\mathbf{H}$ is the $4 \times 4$ PDM defined as

$$\mathbf{H}(f, \delta, \Omega) = (\mathbf{T}^T \otimes \mathbf{R}^T) \cdot \left(\mathbf{R}_F^T \otimes \mathbf{R}_F\right) \tag{5}$$

with ($\otimes$ representing the Kronecker product)

$$\mathbf{T}^T \otimes \mathbf{R}^T = \begin{bmatrix} 1 & \delta_2 & \delta_4 & \delta_2\delta_4 \\ \delta_1 & f_1 & \delta_1\delta_4 & \delta_4 f_1 \\ \delta_3 & \delta_2\delta_3 & f_2 & \delta_2 f_2 \\ \delta_1\delta_3 & \delta_3 f_1 & \delta_1 f_2 & f_1 f_2 \end{bmatrix} \tag{6}$$

and

$$\mathbf{R}_F^T \otimes \mathbf{R}_F = \begin{bmatrix} \cos^2\Omega & \sin\Omega\cos\Omega & -\sin\Omega\cos\Omega & -\sin^2\Omega \\ -\sin\Omega\cos\Omega & \cos^2\Omega & \sin^2\Omega & -\sin\Omega\cos\Omega \\ \sin\Omega\cos\Omega & \sin^2\Omega & \cos^2\Omega & \sin\Omega\cos\Omega \\ -\sin^2\Omega & \sin\Omega\cos\Omega & -\sin\Omega\cos\Omega & \cos^2\Omega \end{bmatrix}. \tag{7}$$

With regard to the problem cardinality, the overall number of unknowns in the most generic PDM calibration problem amounts to 13. More specifically:

- 4 for the complex CI parameters;
- 8 for the complex CT parameters;
- 1 for the real FRA

whereas the number of equations depends on the specific site used for the calibration. In the case of a homogeneous DT, the distortion information can be extracted from the second-order statistics of the observation, i.e., the covariance matrix, in order to exploit further information provided by the data. Depending on the *a priori* information of the target, a few assumptions have been made about its covariances. The most common ones (see [1], [10], and [14]) that will be identically adopted in our analysis are: 1) reciprocity, $S_{\mathrm{VH}} = S_{\mathrm{HV}}$, which is indeed a basic physical property for a monostatic system; and 2) reflection symmetry [18], which is proven to be a solid assumption in most conditions (but not for anisotropic scatterers such as urban areas) [1], [11].

The covariance of the distorted observation then becomes

$$\mathbf{C}_M = A^2 \mathbf{H} \mathbf{C}_S \mathbf{H}^H + \sigma_N \mathbf{I} \tag{8}$$

where $\mathbf{H} = \mathbf{H}(f, \delta, \Omega)$ is the polarimetric distortion matrix, apex $H$ stands for Hermitian transpose, $\sigma_N$ represents the noise contribution, and $\mathbf{C}_S$ is the target covariance that can be modeled, by the assumptions made, as follows:

$$\mathbf{C}_S = E\left[\vec{\mathbf{S}}_{DT} \vec{\mathbf{S}}_{DT}^H\right] = \begin{bmatrix} \sigma_{\mathrm{hh}} & 0 & 0 & \rho^* \\ 0 & \sigma_{\mathrm{hv}} & \sigma_{\mathrm{hv}} & 0 \\ 0 & \sigma_{\mathrm{hv}} & \sigma_{\mathrm{hv}} & 0 \\ \rho & 0 & 0 & \sigma_{\mathrm{vv}} \end{bmatrix} \tag{9}$$

where $\sigma_{\mathrm{hh}} = C_{\mathrm{hh,hh}}$, $\sigma_{\mathrm{hv}} = C_{\mathrm{hv,hv}} = C_{\mathrm{vh,vh}}$, $\sigma_{\mathrm{vv}} = C_{\mathrm{vv,vv}}$, and $\rho = C_{\mathrm{hh,vv}}$. In this case, a total of 16 observables are available (4 real values on the covariance matrix diagonal plus 6 independent out-of-diagonal complex values). However, since $\mathbf{C}_S$ is generally not known in advance, 5 more parameters should be estimated (i.e., the real values $\sigma_{\mathrm{hh}}$, $\sigma_{\mathrm{hv}}$, $\sigma_{\mathrm{vv}}$, and the real and imaginary parts of $\rho$), leading to a total of 16 observables and 18 unknowns, which represents an ill-posed problem. If the radiometric gain $A$ is considered, the number of unknowns will sum up to 19. In our analysis, we will always consider the radiometric gain as a parameter to be estimated since it poses further challenges for the polarimetric calibration, which have been seldom approached in the literature.

The use of a target with known scattering matrix, such as a CR, can be used to increase the number of measures

$$\mathbf{S}_{\mathrm{CR}} = \sqrt{\sigma_{\mathrm{CR}}} \begin{bmatrix} 1 & 0 \\ 0 & 1 \end{bmatrix} \tag{10}$$

where $\sigma_{\mathrm{CR}}$ is the CR radar cross section, which is known *a priori*. The second-order information of the CR can be similarly estimated by resorting to $\mathbf{C}_{\mathrm{CR}} = \vec{\mathbf{S}}_{\mathrm{CR}} \cdot \vec{\mathbf{S}}_{\mathrm{CR}}^H$, where $\vec{\mathbf{S}}_{\mathrm{CR}}$ is the vectorized matrix $\mathbf{S}_{\mathrm{CR}}$.

However, it should be noted that even by adding further observables, the problem is expected to be ill-conditioned.

The ambiguity between CTs + imbalances and Faraday rotation can be evidenced by rewriting the overall Rx matrix (comprehensive of $\delta_1, \delta_2,$ and $f_1$) as the product of a gain factor $k$, a free matrix, and a rotation by an arbitrary angle $\Omega_a$

$$\mathbf{R}_x = \begin{bmatrix} 1 & \delta_2 \\ \delta_1 & f_1 \end{bmatrix} = k \begin{bmatrix} 1 & a \\ b & c \end{bmatrix} \begin{bmatrix} \cos\Omega_a & -\sin\Omega_a \\ \sin\Omega_a & \cos\Omega_a \end{bmatrix}. \tag{11}$$

The second matrix would combine with Faraday rotation getting

$$\begin{aligned} \mathbf{R}_x \mathbf{R}_F &= k \begin{bmatrix} 1 & a \\ b & c \end{bmatrix} \begin{bmatrix} \cos\Omega_a & -\sin\Omega_a \\ \sin\Omega_a & \cos\Omega_a \end{bmatrix} \begin{bmatrix} \cos\Omega & -\sin\Omega \\ \sin\Omega & \cos\Omega \end{bmatrix} \\ &= k \begin{bmatrix} 1 & a \\ b & c \end{bmatrix} \begin{bmatrix} \cos(\Omega+\Omega_a) & -\sin(\Omega+\Omega_a) \\ \sin(\Omega+\Omega_a) & \cos(\Omega+\Omega_a) \end{bmatrix}. \end{aligned} \tag{12}$$

Equation (12) proves that an ambiguity exists between FRA and imbalances + CTs, provided that a complex solution exists for parameters $a, b,$ and $c$, which represent respectively the new ambiguous CTs and the ambiguous imbalance. That solution can be derived by rewriting (12) as follows:

$$\begin{aligned} \mathbf{R}_x \mathbf{R}_F &= k \cdot \cos(\Omega+\Omega_a) \begin{bmatrix} 1 & a \\ b & c \end{bmatrix} \begin{bmatrix} 1 & -t \\ t & 1 \end{bmatrix} \\ &= k_0 \begin{bmatrix} 1 & \frac{a-t}{1+at} \\ \frac{b+ct}{1+at} & \frac{c-bt}{1+at} \end{bmatrix} \end{aligned}$$

where $t = \tan(\Omega + \Omega_a)$, and $k_0$ is an overall scale term that we ignore since it can be incorporated in the radiometric gain. The ambiguous CTs and CI would then be the complex solutions of

$$\delta_2 = \frac{a-t}{1+at}$$

$$\delta_1 = \frac{b+ct}{1+at}$$

$$f_1 = \frac{c-bt}{1+at}.$$

These solutions can be shown to exist for $t \neq 0$, $t \neq 1/\delta_2$, and $\delta_2 \neq \pm 1$. In case $\Omega = 0$, the first ambiguous CT would be for instance

$$a = \frac{t+\delta_2}{1-t\delta_2}$$

that would be strongly biased even for a slight rotation $t$ as $\delta_2$ is usually quite small in amplitude. The same argumentation shall be applied to derive the ambiguous CT and CI in the transmission matrix.

### A. Sensitivity Analysis

A theoretical sensitivity analysis has been conducted on the problem so far delineated to measure the accuracy theoretically achievable by means of numerical optimization. Let us then define $\mathbf{d}$ as the vector containing the real data of the problem and $\mathbf{p}$ as the vector containing the model real parameters (see (13) and (14), shown at the bottom of the next page). For each calibrator set and system distortion setting $\{\mathbf{d}_0, \mathbf{p}_0\}$, the

TABLE I
LIST OF ACRONYMS USED IN THE TEXT

| Acronym | Meaning |
|---|---|
| CI | Channel Imbalance |
| COMET | Covariance Matching Estimation Technique |
| CR | Corner Reflector |
| CT | Cross-talk |
| DT | Distributed Target |
| DWP | Distortion Working Point |
| FRA | Faraday Rotation Angle |
| MNE | Maximum Normalized Error |
| PDM | Polarimetric Distortion Matrix |
| SCR | Signal to Clutter Ratio |

problem well-posedness is investigated by linearizing the system in correspondence of the true values $\mathbf{p}_0$, i.e., by computing the Jacobian $\mathbf{J}$ defined as

$$\delta\mathbf{d} = \mathbf{J}(\mathbf{p}_0) \cdot \delta\mathbf{p}. \tag{15}$$

The singular value decomposition (SVD) of the Jacobian provides information about the feasibility of the problem (through the values of the smallest eigenvalues) and the parameters that are affected by ambiguity and estimation problems (with the analysis of the eigenvector components related to the ill-posed eigenvalues). The feasibility of the full system distortion estimation was evaluated for the case of Faraday rotation not null, to be estimated, with the configuration DT+CR (we already stated that if a DT only is available, the problem is ill-posed). Since the possibility to solve the problem highly depends on the nominal PDM considered, 1000 tests were run on different distortion working points (DWPs; see the other acronyms in Table I), and the average values of the eigenvalues and eigenvectors have been considered (the distortion parameters are randomly chosen in the range of value indicated in Table III). The columns of the matrix model have not been preconditioned in order to get the sensitivity of the single parameters to noise. Fig. 1(a) clearly shows that the problem contains an ambiguity, corresponding to the last eigenvalue, the 19th. The eigenvector components have been then represented (each eigenvector has a number of components corresponding to the number of eigenvalue, which is 19; in case of complex parameters, the average between real and imaginary parts has been considered) and shown in Fig. 1(b), in a 3-D space represented by CI, CT, and FRA and Fig. 1(c)–(f) in the four bidimensional views.

The last eigenvector component (represented in red) spans the null space and is clearly visible in the 2-D plan CI–FRA. We find confirmation of the ambiguity involving Faraday, CT, and in less measure CI, already identified in (11) and (12). It can be noticed, however, that the largest eigenvalue components, in black color, are pointing in Faraday rotation. It means that the parameter is less sensitive to the ambiguity problem with respect to the CT due to the different order of magnitude. An important point to be discussed is whether the knowledge of the FRA rotation may be enough to remove the ambiguity affecting the model. In order to verify it, we performed the same eigenvalue analysis by supposing FRA as given data and not a parameter to be estimated. The results shown in Fig. 1(a) (see the green line) state that if the FRA is known, the ambiguity is removed, even if some criticality may be posed by the high sensitivity to the noise of the lowest eigenvalues. We then investigate the sensitivity of the problem in the case of known FRA.

Let us consider $\mathbf{d}_0$ as the ideal measurement we would have with perfect DT, i.e., infinite number of looks $N_l$, no clutter on the CR, and exact $\Omega_0$ information. We then define $\mathbf{d}(N_l, SCR)$ as the data measurement for finite number of looks $N_l$ and CR quality specified by its signal-to-clutter ratio (SCR), and $\tilde{\mathbf{d}}(N_l, SCR, \Delta\Omega)$ as the measurement in the presence of an extra Faraday error with respect to the true $\Omega_0$, which leads to the deviation $\Delta\mathbf{d} = \tilde{\mathbf{d}} - \mathbf{d}_0$. The model uncertainty $\mathbf{C_p}$ is hence attained by inverting the locally linearized system $\mathbf{J}_0$ after data preconditioning by the weight matrix $\mathbf{W}_0$ according to

$$\Delta\mathbf{p} = \left(\mathbf{J}_0^T\mathbf{W}_0\mathbf{J}_0\right)^{-1}\mathbf{J}_0^T\mathbf{W}_0 \cdot \Delta\mathbf{d} = \mathbf{H}_0 \cdot \Delta\mathbf{d} \tag{16}$$

$$\mathbf{C_p} = \mathbf{H}_0 \cdot \mathbf{C_d} \cdot \mathbf{H}_0^T \tag{17}$$

$$\mathbf{C_p} = \langle \Delta\mathbf{p}\Delta\mathbf{p}^T \rangle, \quad \mathbf{C_d} = \langle \Delta\mathbf{d}\Delta\mathbf{d}^T \rangle \tag{18}$$

$$\mathbf{W}_0 = E\left[(\mathbf{d} - \mathbf{d}_0)(\mathbf{d} - \mathbf{d}_0)^T\right] \tag{19}$$

where $\mathbf{C_d}$ represents the covariance matrix of the small displacements in the recorded data. While the theoretical $\mathbf{W}_0$ is computed through closed-form expressions, $\mathbf{C_d}$ is empirically evaluated by ensemble averaging of the simulated data. In other words, the weights $\mathbf{W}_0$ recall the uncertainty in data measurement that we would expect from our model as a result of a finite $N_l$, whereas $\mathbf{C_d}$ is the actual uncertainty in the data, which differs from $\mathbf{W}_0$ in case of nonnull $\Delta\Omega$.

The theoretical model sensitivity is attained by perturbing the data of several randomly selected DWPs and by averaging the results. The DWP parameter range and the nominal characteristics of the calibrators adopted are those in Table II. The parameter sensitivity is extracted from the diagonal of $\mathbf{C_p}$ and

$$\mathbf{d} = \underbrace{\overbrace{\left[C_{\mathrm{hh}}^{DT} \cdots C_{\mathrm{vv}}^{DT}, \mathcal{R}\left(C_{\mathrm{hh,hv}}^{DT}\right), \mathcal{I}\left(C_{\mathrm{hh,hv}}^{DT}\right) \cdots \mathcal{I}\left(C_{\mathrm{hh,vv}}^{DT}\right),\right.}^{\text{DT only}} \left. C_{\mathrm{hh}}^{CR} \cdots \mathcal{I}\left(C_{\mathrm{hh,vv}}^{CR}\right)\right]^T}_{\text{DT+CR}} \tag{13}$$

$$\mathbf{p} = \underbrace{\overbrace{[A, |f_1|, \angle f_1, |f_2|, \angle f_2, |\delta_1|, \angle\delta_1, \cdots |\delta_4|, \angle\delta_4, \sigma_{\mathrm{hh}}, \sigma_{\mathrm{hv}}, \sigma_{\mathrm{vv}}, \mathcal{R}(\rho), \mathcal{I}(\rho)}^{\text{system}}, \Omega]^T}_{\text{system+FRA}} \tag{14}$$

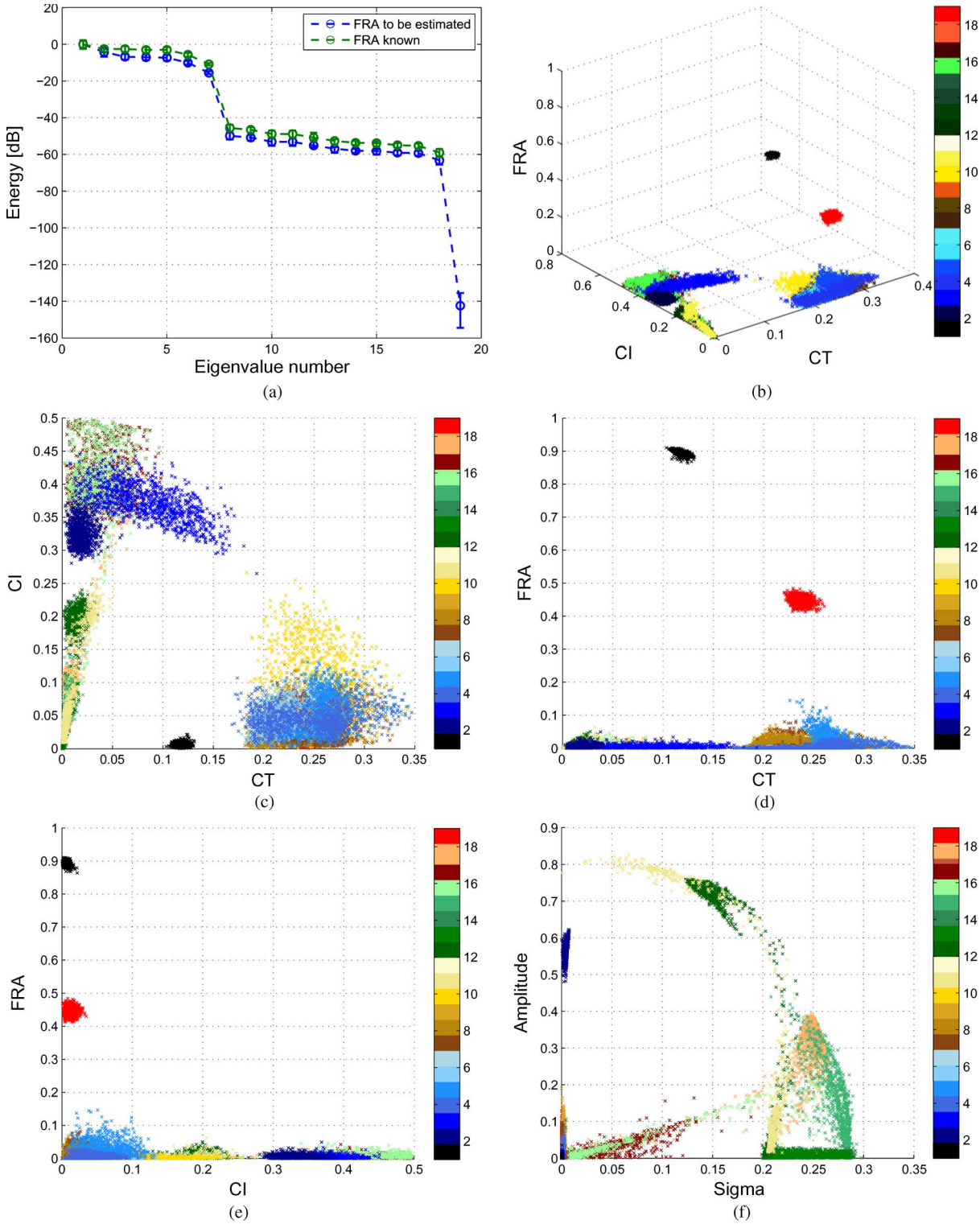


Fig. 1. Eigenvalues and eigenvectors obtained after 1000 random SVD decompositions. (a) Eigenvalues. (b) Eigenvector values for CI, CT, and FRA. Each point is associated with the related eigenvector component, whose number is specified by the color. (c) Two-dimensional view in the CI–CT plan. (d) Two-dimensional view in the CT–FRA plan. (e) Two-dimensional view in the CI–FRA plan. (f) Two-dimensional view in the DT–absolute calibration factor plan.

allows to understand how the single parameters are influenced by small displacements of the data, i.e., because of noise. For example, following the notations of (14) and (18), the first value of the diagonal provides an estimate of the sensitivity of the absolute gain, the second and third of $f_1$ amplitude and phase, values 3 and 4 provide an estimate of the sensitivity of $f_2$ amplitude and phase, and so on, up to the last value that represents the sensitivity of the Faraday rotation (in case it has to be estimated) or the imaginary part of the $\rho$ parameter. The results of the analysis are shown in the experimental section and compared with those obtained with the proposed COMET optimizer, as a comparison for correctness of the method.

TABLE II
PARAMETERS CONSIDERED TO CREATE THE SYNTHETIC DATA SETS

| Parameters | | Unit | Value |
|---|---|---|---|
| DT | RCS ($\sigma_{hh}, \sigma_{hv}, \sigma_{vv}$) | [dB] | 0 / -6.5 / 0 |
| | $\rho$ | [lin] | $0.4 \angle 10°$ |
| | SNR (HH,HV,VH) | dB | 20 /13.5 / 20 |
| | Number of looks | - | $10^5$ |

## III. COMET APPROACH FOR POLARIMETRIC CALIBRATION

The use of various numerical optimizers for polarimetric calibration was recently proposed in the literature (see [15], [19], and [20]). One optimizer not yet proposed, the COMET algorithm, provides a least squares solution and ensures the asymptotic optimality [16]. For this reason, we propose in this paper a COMET-based approach to estimate the polarimetric distortion parameters. COMET is an interesting alternative to maximum-likelihood estimators since it provides similar properties with a generally lower computational cost [21]. In the literature, it was shown that covariance matching approaches are well suited to solve a large number of problems related to signal processing [16], [22].

The first step for the optimization process is represented by the definition of the values of all the parameters indicated by (14). Once the parameters are defined, we can compute matrices $\mathbf{H}$ and $\hat{\mathbf{C}}_S$, defined respectively by (5) and (9), and consequently estimate the expected covariance $\mathbf{C}_{\text{inv}}$ for a given distortion parameter configuration, according to the following equation:

$$\mathbf{C}_{\text{inv}}(\hat{f}, \hat{\delta}, \hat{\sigma}, \hat{\rho}, \Omega_{\text{est}}) = \mathbf{H}(\hat{f}, \hat{\delta}, \Omega_{\text{est}}) \cdot \hat{\mathbf{C}}_S(\hat{\sigma}, \hat{\rho}) \cdot \mathbf{H}^H(\hat{f}, \hat{\delta}, \Omega_{\text{est}}) + \sigma_N \mathbf{I}. \quad (20)$$

Parameters $\hat{f}, \hat{\delta}, \hat{\sigma},$ and $\hat{\rho}$ represent the estimate of the optimizer, whereas $\Omega_{\text{est}}$ is the FRA value externally provided. If the problem is not ambiguous (please refer to Section II for the feasibility study), an exact matching between the expected covariance $\mathbf{C}_{\text{inv}}$ and the covariance computed from the data is possible only if these parameters are correctly estimated. Following this statement, the error metric considered for the optimizer is given by the following function (we omit the dependence for notational convenience):

$$e = \left\| \mathbf{W}^{-1/2} \cdot (\vec{\mathbf{C}}_{\text{data}} - \vec{\mathbf{C}}_{\text{inv}}) \right\| \quad (21)$$

which takes into account the error between the reconstructed covariance $\mathbf{C}_{\text{inv}}$ and the measured sample covariance matrix (SCM) $\mathbf{C}_{\text{data}}$ with the weighting function $\mathbf{W}$, representing the covariance matrix of the SCM elements, expressing the uncertainty due to the limited number of looks in its computation. The weighting function is computed following the formulation of [16]:

$$\mathbf{W} = \frac{1}{N} \cdot \left( \mathbf{C}_{\mathbf{data}}^T \otimes \mathbf{C}_{\mathbf{data}} \right). \quad (22)$$

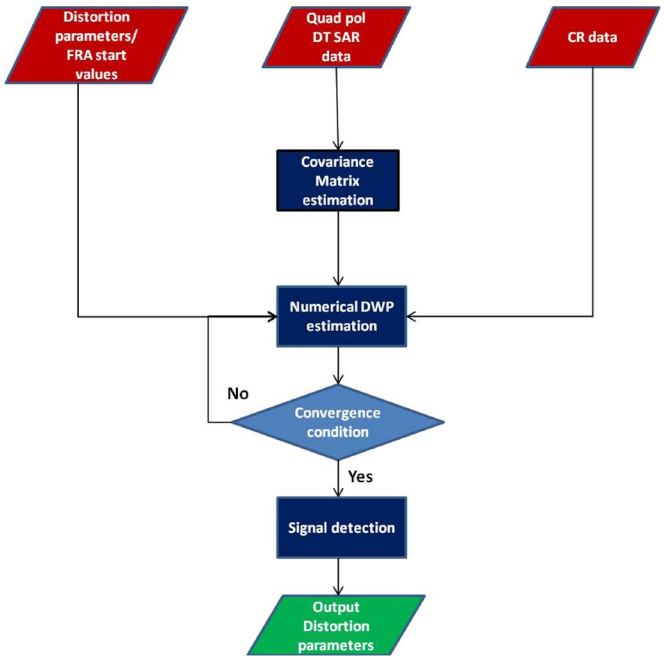


Fig. 2. Block diagram of the proposed numerical optimizer.

The parameter final estimates are then readily obtained by moving toward the $e$ minimum with the use of a Hessian optimizer, i.e., with the following formula:

$$\hat{f}, \hat{\delta} = \arg\min_{\mathbf{H}(\hat{f}, \hat{\delta}, \Omega_{\text{est}}), \mathbf{C}_S(\hat{\sigma}, \hat{\rho})} \times \left\| \mathbf{W}^{-1/2} \cdot \left( \vec{\mathbf{C}}_{\text{data}} - \vec{\mathbf{C}}_{\text{inv}}(\mathbf{H}, \mathbf{C}_S) \right) \right\| \quad (23)$$

leading to the final output of the numerical optimizer.

The overall scheme of the proposed COMET-based approach is depicted in Fig. 2. The method exploits the information provided by both a DT and a passive CR. Given the input data, the following are the five main steps of the method.

- SCM computation: First, the SCM of the considered DT is computed. This step is needed to obtain the covariance measures that have to be used for the cost function and the weights computation. Similarly, the contribution of the CR is estimated.
- Model initialization: The model is then initialized by the starting DWP parameters, for example, those provided by internal calibration. It should be noted that the ambiguity between Faraday rotation and CT requires the prior knowledge of the FRA or its computation with the assumption of a calibrated image (leading to an approximate FRA value if the assumption is not verified).
- Cost function computation: The cost function is computed by considering (21).
- Distortion working parameter (DWP) computation: The results of the computation are given as input to the numerical optimizer, which iterates until the parameters that minimize the cost function are found, both for the polarimetric distortion and the covariance matrix of the DT.

TABLE III
VALUES CONSIDERED TO CREATE THE DISTORTION WORKING PARAMETERS

| Parameter | | Unit | Value |
|---|---|---|---|
| Amplitude | Channel imbalance | [dB] | [-3 3] |
| | Cross-talks | [dB] | [-27 -35] |
| | Faraday Rotation | [deg] | [0 20] |
| Phase | Channel imbalance | [deg] | [-20 20] |
| | Cross-talks | [deg] | [-180 180] |

- Block detection: Block detection is finally performed. The assumption is that data with wrong results (i.e., not satisfying the assumptions of the model) will show a high cost function. Therefore, after dividing an image into different blocks and estimating the distortion parameters of each block, the unreliable results (e.g., with cost function higher than a given threshold) are discarded.

The final output is the complete set of polarimetric distortion parameters required.

## IV. EXPERIMENTS ON SYNTHETIC DATA

### A. Synthetic Data Set Creation

Experiments on data synthetically generated are performed in order to validate the proposed algorithm. Given the input parameters specified in Table II, the procedure to build the synthetic data set is as follows:

— Generation of the data set according to the number of points, backscatter coefficients, and co-polarization/cross-polarization signal-to-noise ratio.
— Creation of DWP and application to the data. The values are randomly selected in the range specified in Table III.
— Generation of thermal noise and addition to the data set.

It should be noted that recent works have shown that the CTs can have values lower than those indicated in Table III (see, for example, [2] and [11]). However, several papers in the literature suggest that if the CTs have very small values (for example, indicated values smaller than $-35$ dB), they can be neglected since there is a high probability to have wrong estimations related to noise [14] and, we add, to the Faraday ambiguity itself. In this test, we are interested in the investigation of the ability of the numerical optimizer to correctly estimate the CTs when they can produce significant changes in the scene. Preliminary tests have shown that when the CTs have values smaller than $-35$ dB, the proposed numerical optimizer estimates very low values of CT gain, confirming the results, which will be illustrated in the following.

### B. Indexes Considered for Performance Assessment

In order to evaluate the ability of the method to perform a polarimetric calibration, two complementary indicators can be considered. From the viewpoint of the system characteristic, each distortion parameter should be evaluated. The metric adopted here is the root-mean-square error (RMSE), evaluated for the gain expressed in decibels and the phases expressed in degrees. However, in the presence of Faraday rotation, the distortion matrix is ambiguous, as discussed in Section II. In this case, it would be better to use the maximum normalized error (MNE) [23]

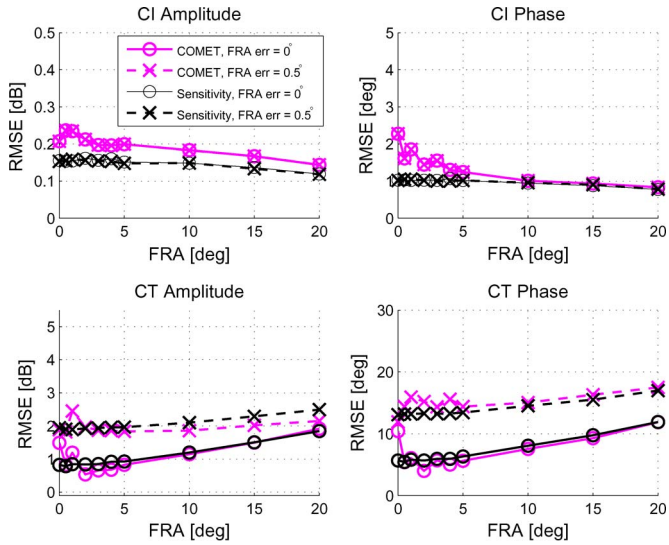


Fig. 3. Parameter estimate RMSE, DT + CR configuration. DT with $10^5$ points, SNR = 20 dB co-polarization. CR SCR = 26 dB. (Magenta) COMET with DT + CR information (continuous line: exact FRA value; dashed line: FRA error = 0.5°). (Black) Sensitivity analysis (continuous line: exact FRA value; dashed line: FRA error = 0.5°). CIs = channel imbalances, CT = crosstalks, and FRA = Faraday rotation angle.

$$\text{MNE} = \sqrt{\lambda_{\max} \cdot \left[\mathbf{A}_4^T \cdot (\mathbf{H}-\mathbf{I})^H \cdot (\mathbf{H}-\mathbf{I}) \cdot \mathbf{A}_4\right]} \quad (24)$$

where $\mathbf{H}$ represents the polarimetric distortion matrix, $\mathbf{I}$ is the identity matrix, $\lambda_{\max}$ stands for the largest eigenvalue of the enclosed matrix $[\mathbf{A}_4^T \cdot (\mathbf{H}-\mathbf{I})^H \cdot (\mathbf{H}-\mathbf{I}) \cdot \mathbf{A}_4]$, and $\mathbf{A}_4$ is a binary $4 \times 3$ matrix as follows:

$$\mathbf{A}_4 = \begin{bmatrix} 1 & 0 & 0 \\ 0 & 1 & 0 \\ 0 & 1 & 0 \\ 0 & 0 & 1 \end{bmatrix}. \quad (25)$$

This metric is only related to the system characteristics. The index can be conveniently rephrased to compute the worst case error in case of polarimetric distortion by substituting the identity matrix (corresponding to the case where no distortion is present) with the estimated polarimetric distortion matrix, leading to the index adopted in this paper:

$$\text{MNE} = \sqrt{\lambda_{\max} \cdot \left[\mathbf{A}_4^T \cdot (\mathbf{H}-\mathbf{H}_{\mathbf{est}})^H \cdot (\mathbf{H}-\mathbf{H}_{\mathbf{est}}) \cdot \mathbf{A}_4\right]}. \quad (26)$$

All the parameters have the same meaning as in (24), the only difference being that the identity matrix $\mathbf{I}$ has been substituted by the polarimetric distortion matrix $\mathbf{H}_{\mathbf{est}}$ estimated.

### C. Results

The experiment on synthetic data was performed by considering the information of a DT plus a known point target (i.e., a CR). The DT is a rainforest type, and the parameters characterizing it are shown in Table II. The SCR of the CR is set to

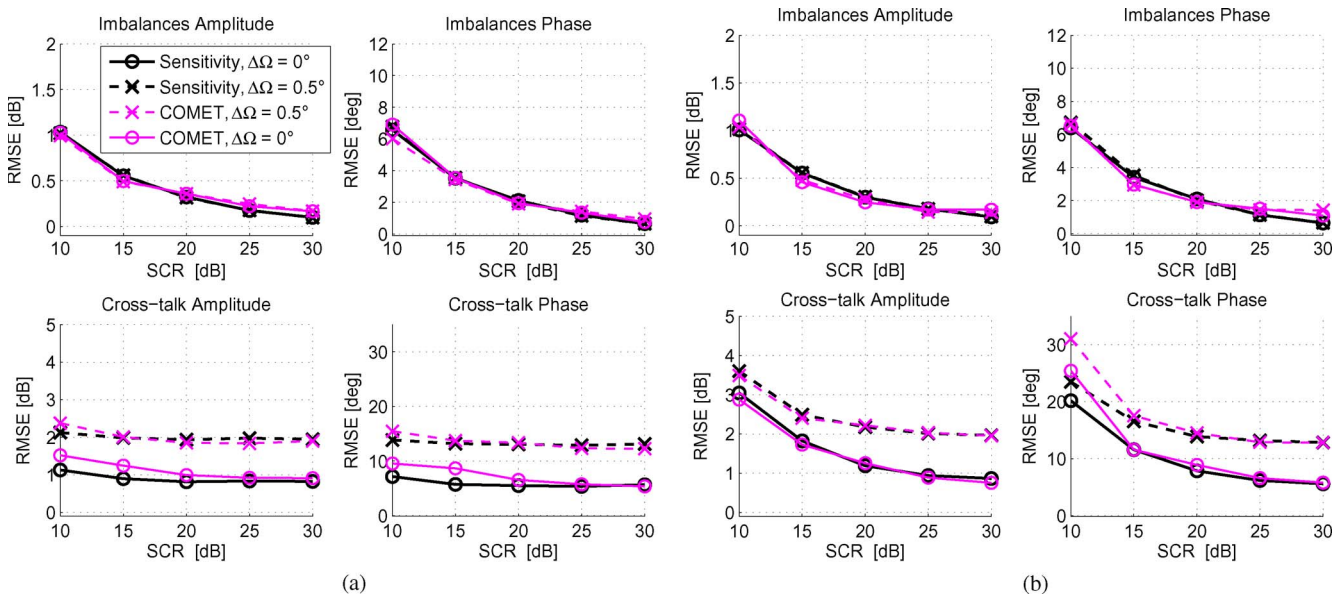


Fig. 4. Parameter estimate RMSE, DT + CR. (a) FRA $= 0°$. (b) FRA $= 5°$. (Magenta) COMET with DT + CR information (continuous line: exact FRA value; dashed line: FRA error $= 0.5°$). (Black) Sensitivity analysis (continuous line: exact FRA value; dashed line: FRA error $= 0.5°$). CIs = channel imbalances. CT = crosstalks.

26 dB, which appears to be a realistic value for a CR deployed for an L-band satellite. Several Faraday rotation values tested from 0° to 20° and for each FRA value, 200 experiments with different configurations of polarimetric distortion parameters were tested (in the range of values shown in Table III). The proposed numerical optimizer using the information of a DT + CR (both in case of known FRA or in the case of approximated value with average error of 0.5°) is compared with the results of the sensitivity study presented in Section II. The results are shown in Fig. 3. Several interesting conclusions can be drawn from the first experiment. First, the information provided by a DT plus a CR is able to provide reasonable estimates of the parameters, even with an approximated estimate of the Faraday rotation. Regarding the system distortion parameters, the use of an approximated value of Faraday rotation does not affect the estimate of the CI (both in gain and phase). On the other hand, a larger error is noticed for the CT estimates, even if the RMSE is well below 3 dB in amplitude and around 20° in phase, which are fair results for the CT values. The larger error is caused by the ambiguity previously shown in Fig. 1.

The second test is devoted to the assessment of the importance of the quality of the CR for the parameter estimation. The influence of noise on the achievable results has been tested by considering several values of signal-to-clutter ratio between 10 and 30 dB (with a fix signal-to-noise ratio of 20 dB for the co-polarization channels of the DT). The results are shown in Fig. 4 for two different values of Faraday rotation, i.e., 0° and 5°. The average value for each system polarimetric distortion parameter is shown (i.e., CT gain and phase). The results confirm the study performed with the sensitivity analysis: The CI estimation does not suffer from an approximated value of Faraday rotation on the order of 0.5°, whereas the CTs are much more sensitive. However, even in case of low SCR, the CT estimates show reasonable errors. In case of FRA $= 5°$, the maximum error is 4 dB, whereas in case of null FRA, the maximum error is 2 dB. The results obtained by the optimizer tend to the optimal value indicated by the sensitivity study, with very small bias caused by small differences caused mainly by the nonideality in the DT weights in (22), which is based on the perturbed data, and by convergence issues of the numerical solve, therefore confirming the ability of the proposed approach to obtain the best solution.

Finally, the quality of the calibration is analyzed through the MNE. The results are shown in Fig. 5. As for the CI and CT, the MNE largely depends on the quality of the CR that is considered. In case of good-quality CR, the MNE is almost constant independently of the FRA value. It is important to notice that, no matter of the FRA and SCR, an error in the FRA value externally provided to the optimizer does not lead to worsening of the MNE value since the retrieved PDM is the same in both cases. As a summary of this section, we can conclude that when the problem is well conditioned, the proposed method is able to retrieve the best solution, as stated by the comparison with the sensitivity study results. An error of 0.5° in the FRA externally provided (which is a reasonable accuracy value expected from FRA estimation) leads to a decrease in the CT accuracy but does not affect the CI retrieval. Moreover, we can conclude that, when trying to estimate the PDM rather than each distortion parameter, it is not necessary to know the exact value of Faraday rotation since the MNE values obtained in the case of approximated FRA are the same as those obtained with the exact value.

### *D. Algorithm Convergence*

We investigate the ability of the numerical optimizer to solve the calibration problem, given different starting point errors for the parameters. The value of the Faraday rotation is fixed in order to obtain a univocal solution, and no noise is considered. Please notice that the test is devoted to the investigation of the

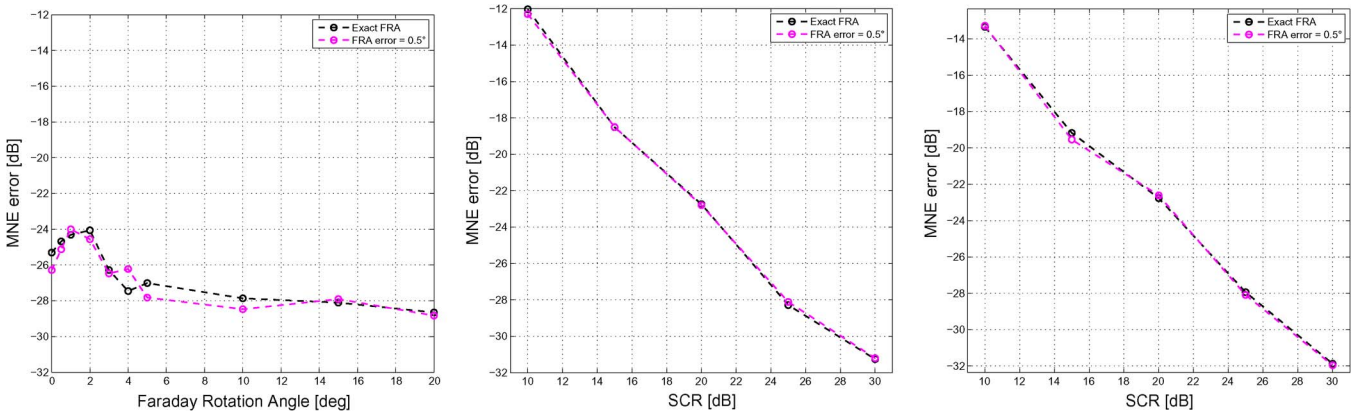


Fig. 5. MNE. (Left) SCR $= 26$ dB. (Center) FRA $= 0°$. (Right) FRA $= 5°$. COMET with DT + CR information (black line: exact FRA value; magenta line: FRA error $= 0.5°$).

convergence of the algorithm (i.e., if the algorithm is able to retrieve the solution, when the problem is well conditioned) and not the performances in case of noise or FRA retrieval error. Because of this reason, we have considered the FRA value as known *a priori* so that a unique solution exists. The test setup is the following: The system polarimetric distortion parameters were randomly chosen in the range shown in Table III, for a total of 1000 simulations so that a large number of different configurations can be tested. Different values of starting point errors have been tested for the parameters, with the assumption that the starting error of all the parameters is proportional. The reason for this assumption is to ensure the independence of the parameter retrieval, i.e., if the optimizer will receive in input a CT with very low starting error and CIs with very large errors, it will likely produce a wrong estimation of the CTs due to the different conditions of the PDM. However, this error should not be related to the initial CT starting error, rather to the whole PDM starting error. The test is conducted by considering a DT plus a CR. The results in Fig. 6 show that the algorithm is robust, providing a correct estimate even in the case of very large initial errors. All the parameters that have to be optimized converge to the final solution independently of the starting point.

### E. Result Detection

In order to verify the reliability of the obtained solution, a detection must be performed. The detection aims at finding a parameter related to the quality of the solution and defining a threshold for the parameter. If the detection parameter is larger than the defined threshold, the solution is considered as unreliable.

Ottersten *et al.* proposed for the COMET approach a detection technique based on the optimized cost value, which has proven to be robust when compared to other indicators as the well-known generalized-likelihood ratio [16]. Fig. 7(a) shows the relationship between the final cost value and the MNE, obtained from the all the experiments conducted on the synthetic data (based on the verified assumption that similar cost values correspond to similar MNE value, independently of the experiment). The direct relationship between these two quantities is clear, confirming that a low cost function provides a lower MNE solution and therefore stating the suitability of the cost value to be used for result detection.

The second point to be addressed is the selection of a reasonable threshold $E_{\text{th}}$ to define which solutions can be considered as reliable, according to the following relation:

$$e \lessgtr_{H_0}^{H_1} E_{\text{th}} \tag{27}$$

where $E_{\text{th}}$ is the threshold indicating if a solution is acceptable or not, $H_1$ is the case of an acceptable solution (i.e., cost value smaller than selected threshold), and $H_0$ is the case of a solution to be rejected (cost value larger than selected threshold).

To select a proper threshold for the solution detection, we build the theoretical relationship between the MNE and the COMET cost function by considering different values of CIs.

Based on the results exposed in [23], the MNE suggested for a good calibration corresponds to $-20$ dB. This result is equivalent to 0.3 dB of residual CI gain and $2°$ of phase (as stated in [23]). To define a proper threshold for detection, we build the probability of good calibration for a given cost, considering a data set well calibrated if the resulting MNE is lower than $-20$ dB. Fig. 7(b) shows the results obtained for different cost values. For example, for a probability of good calibration larger than 80%, the cost value for the detection should be lower than 500.

## V. Experiments on Real Data

The final experiment is conducted on a real data set, acquired by the L-band satellite PALSAR. The stack includes 11 full polarimetric level-1.1 images acquired between 2006 and 2010. The data were acquired over the area around Munich and contain both urban areas and agricultural fields. Full polarimetric products, i.e., PALSAR products, (i.e., PLR L1.1 and PLR L1.5 products) are provided with CT and CI corrected, whereas Faraday rotation is not removed. The stability of the methodology is therefore investigated in this test. Since no CR or other known targets are present in the image, the full set of parameters cannot be estimated. The values of two CTs are set to the values obtained with the technique [10] (which are on the order of $-40$ dB); hence, the algorithm is able to retrieve

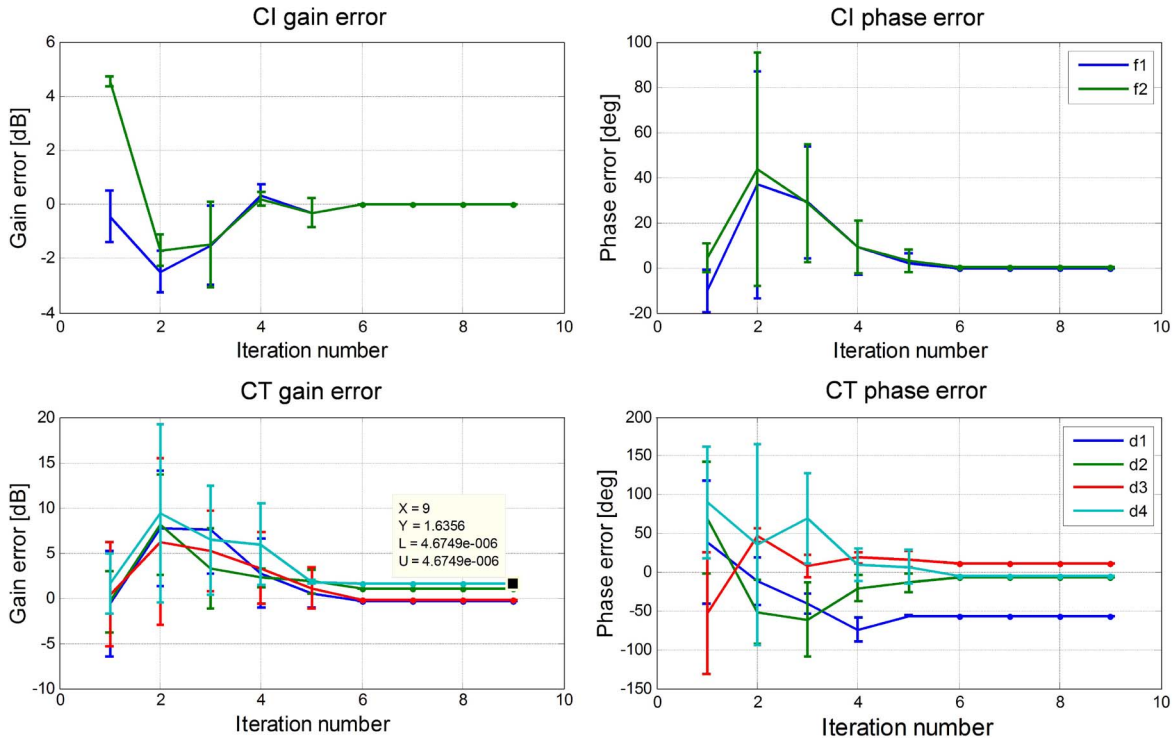


Fig. 6. Convergence of the numerical optimizer in the case of DT + CR: RMSE (average and standard deviation) versus number of iterations.

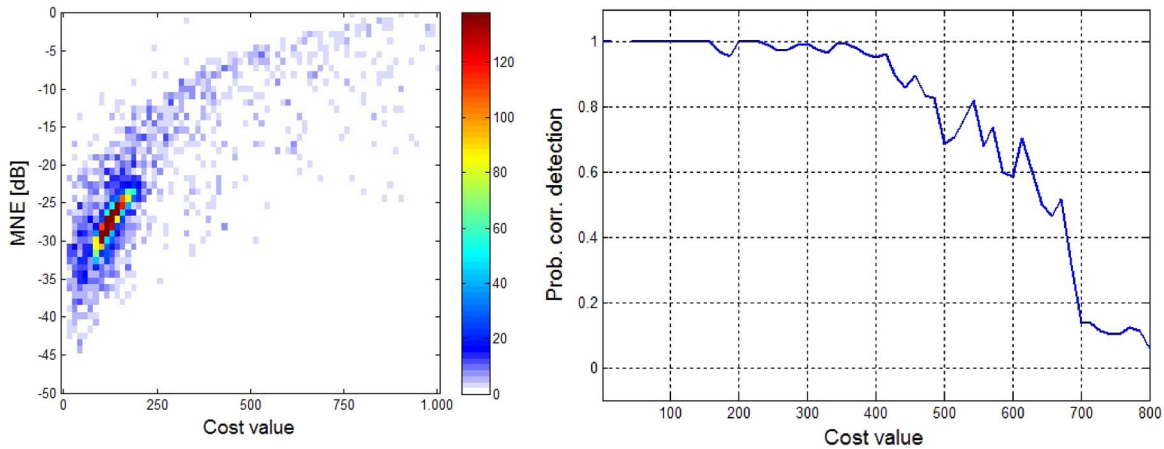


(a) (b)

Fig. 7. (a) Relationship between COMET cost function obtained at the end of optimization and MNE. (b) Probability of correct calibration (that is considered as MNE $< -20$ dB.)

without ambiguities the remaining parameters by considering a DT only. Each scene is divided into 552 blocks (46 azimuth times 12 range blocks, each of dimension 400 $\times$ 100 pixels), and the optimizer is run on each single block. As it shown in Fig. 8, the areas not occupied by a DT (i.e., the center-left urban areas), show higher values of CTs since the assumptions of the model are not verified. This problem is reflected in a higher COMET cost obtained at the end of the optimization.

Fig. 9 shows the bidimensional histograms relating the CT gains with the COMET cost. It can be noticed that low cost values (corresponding to a good optimization index) correspond to very low CT values and a lower estimate dispersion. As previously stated in [16], we have verified also that the generalized-likelihood ratio leads to similar conclusions, and therefore, we have adopted the COMET cost function as a detection. Looking at Fig. 9, the value of 200 appears to be a reasonable threshold for the parameter detection. The average results of the parameters estimated for each image after the detection are shown in Fig. 10. It can be noticed that, as expected, the CTs are below $-40$ dB in all the cases. The CI values are close to one, whereas the phases show small variations around $0^\circ$. The differences with respect to the calibrated conditions (CIs equal to one with null phase) are expected to be caused by a misalignment between the nominal polarimetric correction factor used by the processor to calibrate the data and the real values of the sensor.

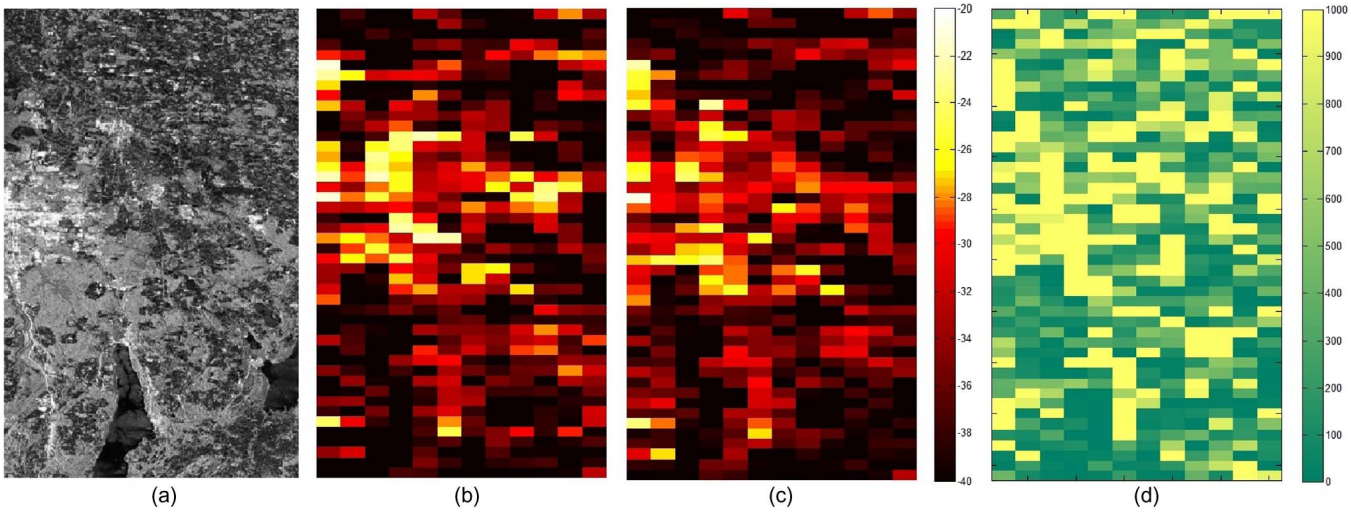


Fig. 8. (a) PALSAR image #1 HH polarization acquired around the area of Munich. (b) CT #3 estimates obtained by the numerical optimizer. (c) CT #4 estimates obtained by the numerical optimizer. (d) Cost function obtained at the end of the optimization.

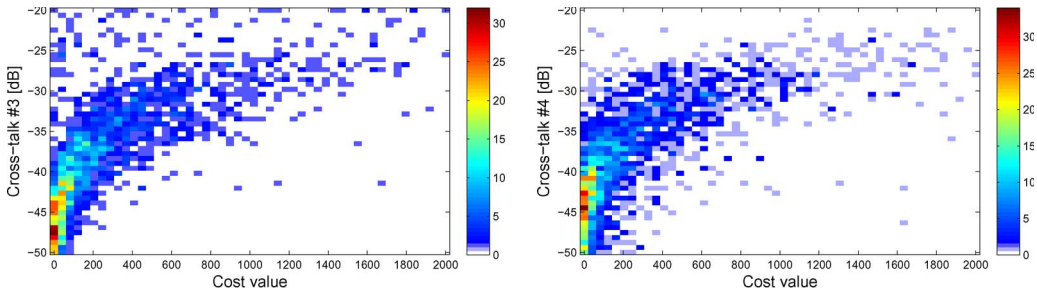


Fig. 9. Histogram relating CT gains and COMET cost at the end of the optimization. (Left) CT #3. (Right) CT #4.

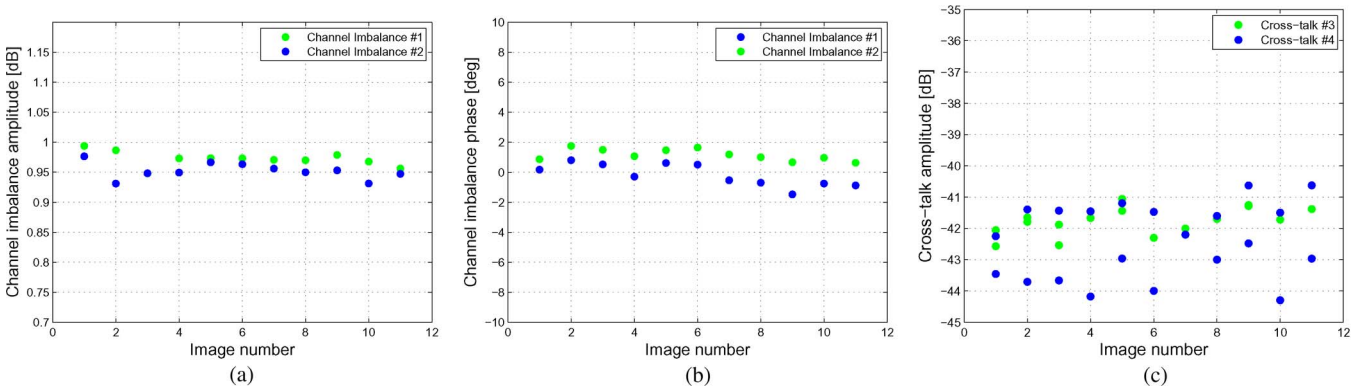


Fig. 10. System parameter values obtained at the end of the optimization for each image. (a) CI amplitude. (b) CI phase. (c) CT amplitude. Blue and green represents the two values obtained (CIs #1 and #2–CTs #3 and #4).

## VI. Conclusion

The problem of polarimetric data calibration and system monitoring for retrieval of distortion parameters has been investigated in this paper. The retrieval of distortion parameters from fully polarimetric data has been first discussed from a theoretical point of view and then approached by an innovative numeric method, based on the statistically optimal covariance matching. The ambiguity affecting the distortion parameters has been completely identified in the nonlinear problem and confirmed by the systematic eigenvalue analysis of the forward problem, based on linearization for ten thousands different working points. The ambiguity, involving Faraday rotation and CTs, and in lower measure CIs, cannot be solved but by assuming *a priori* information.

The following conclusions can be drawn.

— The ambiguity is not relevant as for calibration but prevents proper monitoring of the acquisition parameters, for example, CT cannot be univoquely estimated from data unless specific configurations are given (like for symmetric CT or known FRA).

— Faraday rotation is less affected by the ambiguity with respect to CTs due to the different order of magnitude, as shown by the first eigenvector whose associated eigenvalue is better than all the others. On the other hand, the slightest uncertainty in FRA completely jeopardizes the estimate of CT.
— CTs and CIs can be estimated, from DT and CR, with a sensitivity that is 8–10 dB lower.

The theoretical analysis clearly determined the need for robust *a priori* information to remove the ambiguity of the problem. Consequently, the sensitivity of the estimation of each element of the PDM has been then derived in some conditions of interest, where the ambiguity has been removed. A novel numerical method, based on covariance matching, was proposed to estimate the PDM and then perform polarimetric calibration. The method has proven to be robust and converging with all the starting points usually assumed. The method does not need any approximation about Faraday rotations (small/large) and has an accuracy value that compares with the theoretical sensitivity derived from the linearized analysis. The stability of measures, verified on real data, has been found consistent with the results obtained with the analysis of synthetic data.

## ACKNOWLEDGMENT

The authors would like to thank Prof. F. Rocca for the contribution to the work, particularly for the fruitful discussions on the model conditioning and sensitivity. They would also like to thank the reviewers for comments that led to better investigation of the theoretical analysis of the problem.

## REFERENCES

[1] S. Quegan, "A unified algorithm for phase and crosstalk calibration of polarimetric data-theory and observations," *IEEE Trans. Geosci. Remote Sens.*, vol. 32, no. 1, pp. 89–99, Jan. 1994.
[2] R. Touzi and M. Shimada, "Polarimetric PALSAR calibration," *IEEE Trans. Geosci. Remote Sens.*, vol. 47, no. 12, pp. 3951–3959, Dec. 2009.
[3] R. Touzi, R. K. Hawkins, and S. Coté, "High-precision assessment and calibration of polarimetric RADARSAT-2 SAR using transponder measurements," *IEEE Trans. Geosci. Remote Sens.*, vol. 51, no. 1, pp. 487–503, Jan. 2013.
[4] K. Sarabandi, "Calibration of a polarimetric synthetic aperture radar using a known distributed target," *IEEE Trans. Geosci. Remote Sens.*, vol. 32, no. 3, pp. 575–582, May 1994.
[5] H. Kimura, T. Mizuno, K. Papathanassiou, and I. Hajnsek, "Improvement of polarimetric SAR calibration based on the quegan algorithm," in *Proc. IEEE IGARSS*, Sep. 2004, vol. 1, pp. 186–187.
[6] C. Lopez-Martinez, A. Cortes, and X. Fabregas, "Analysis and improvement of polarimetric calibration techniques," in *Proc. IEEE IGARSS*, Jul. 2007, pp. 5224–5227.
[7] A. Freeman and S. Saatchi, "On the detection of Faraday rotation in linearly polarized L-band SAR backscatter signatures," *IEEE Trans. Geosci. Remote Sens.*, vol. 42, no. 8, pp. 1607–1616, Aug. 2004.
[8] J. Kim and K. Papathanassiou, "Faraday rotation estimation performance analysis," in *Proc. EuSAR*, 2010, pp. 1–4.
[9] J. Chen and S. Quegan, "Improved estimators of Faraday rotation in spaceborne polarimetric SAR data," *IEEE Geosci. Remote Sens. Lett.*, vol. 7, no. 4, pp. 846–850, Oct. 2010.
[10] A. Freeman, X. Pi, and B. Chapman, "Calibration of PALSAR polarimetric data," in *Proc. 4th Int. Workshop Sci. Appl. PolInSAR*, Apr. 2009, pp. 668–672.
[11] M. Shimada, "Model-based polarimetric SAR calibration method using forest and surface-scattering targets," *IEEE Trans. Geosci. Remote Sens.*, vol. 49, no. 5, pp. 1712–1733, May 2011.
[12] P. Wright, S. Quegan, N. Wheadon, and C. Hall, "Faraday rotation effects on L-band spaceborne SAR data," *IEEE Trans. Geosci. Remote Sens.*, vol. 41, no. 12, pp. 2735–2744, Dec. 2003.
[13] J. Chen, S. Quegan, and X. Yin, "Calibration of spaceborne linearly polarized low frequency SAR using polarimetric selective radar calibrators," *Progr. Electromagn. Res.*, vol. 114, pp. 89–111, 2011.
[14] A. Freeman, "Calibration of linearly polarized polarimetric SAR data subject to Faraday rotation," *IEEE Trans. Geosci. Remote Sens.*, vol. 42, no. 8, pp. 1617–1624, Aug. 2004.
[15] A. Takeshiro, T. Furuya, and H. Fukuchi, "Verification of polarimetric calibration method including Faraday rotation compensation using PALSAR data," *IEEE Trans. Geosci. Remote Sens.*, vol. 47, no. 12, pp. 3960–3968, Dec. 2009.
[16] B. Ottersten, P. Stoica, and R. Roy, "Covariance matching estimation techniques for array signal processing applications," *Digit. Signal Process.*, vol. 8, no. 3, pp. 185–210, Jul. 1998.
[17] S. Tebaldini, F. Rocca, and A. Monti Guarnieri, "Model based SAR tomography of forested areas," in *Proc. IEEE IGARSS*, 2008, vol. 2, pp. 590–593.
[18] S. V. Nghiem, S. H. Yueh, R. Kwok, and F. K. Li, "Symmetry properties in polarimetric remote sensing," *Radio Sci.*, vol. 27, no. 5, pp. 693–711, Sep./Oct. 1992.
[19] W. Xiong, "Polarimetric calibration using a genetic algorithm," *IEEE Geosci. Remote Sens. Lett.*, vol. 4, no. 3, pp. 421–425, Jul. 2007.
[20] H. Kimura, "Calibration of polarimetric PALSAR imagery affected by Faraday rotation using polarization orientation," *IEEE Trans. Geosci. Remote Sens.*, vol. 47, no. 12, pp. 3943–3950, Dec. 2009.
[21] T. W. Anderson, *An Introduction to Multivariate Statistical Analysis*, vol. 2. New York, NY, USA: Wiley, 1958.
[22] M. Bengtsson and B. Ottersten, "Low-complexity estimators for distributed sources," *IEEE Trans. Signal Process.*, vol. 48, no. 8, pp. 2185–2194, Aug. 2000.
[23] Y. Wang, T. Ainsworth, and J.-S. Lee, "Assessment of system polarization quality for polarimetric SAR imagery and target decomposition," *IEEE Trans. Geosci. Remote Sens.*, vol. 49, no. 5, pp. 1755–1771, May 2011.